A Numerical Study of Penetration in Concrete Targets by Eroding Projectiles of Different Materials

S. Harikrishnan[#,*], V. Venkateswara Rao[#], and Ajay Misra[@]

[#]*DRDO-Armament Research and Development Establishment, Pune - 411 021, India*
[@]*DRDO-Department of Aerospace Engineering, Defence Institute of Advanced Technologies, Pune - 411 025, India*
[*]*E-mail: sharikrishnan@arde.drdo.in*

ABSTRACT

Numerical simulations have been performed to examine the effect of three different eroding rod materials on the penetration in concrete targets. Same kinetic energy is delivered to concrete target using cylindrical rods of Aluminium, Iron, and Copper of identical size. Impact velocities have been varied to keep the kinetic energy the same. Penetration characteristics like centerline interface velocity, penetrator deceleration, plastic strain in the target, and energy partitioning during penetration have been studied for the three different penetrator materials. In all three cases, penetration proceeds nearly hydrodynamically. It is seen that even though the steady-state penetration ceases before reaching the hydrodynamic limit, the secondary penetration takes the total penetration beyond the hydrodynamic value. Plastic strain in the target material is a measure of damage beyond the crater produced by penetration. The lateral extent of plastic strain in target is more for Aluminium penetrator compared to the other two. Energy partitioning during penetration provides details of the rate at which energy is entering into the target. Kinetic energy delivered to the target during impact is partitioned into internal energy and kinetic energy of the target. Finally, the influence of target thickness on the extent of plastic strain has been studied. The result shows that Aluminium penetrators inflict maximum damage to targets of finite thickness.

Keywords: Concrete penetration; Hydrocode simulation; Eroding projectile; Energy partitioning

NOMENCLATURE

ρ_p	Penetrator density
ρ_t	Target density
v	Penetrator impact velocity
u	Penetration velocity
Y_p	Flow stress in projectile
R_t	Target resistance
p	Penetration depth
l	Penetrator length
p_{tot}	Total penetration
L	Initial length of penetrator
S_h	Hydrodynamic limit
σ_{eq}	Equivalent flow stress
ε_p	Effective plastic strain
$\dot{\varepsilon}_p$	Effective plastic strain rate
θ	Homologous temperature
T_m	Melting temperature
η	Compression ratio
T	Temperature
E_{KIN}	Kinetic Energy
E_{INT}	Internal Energy
E_{TOT}	Total Energy

1. INTRODUCTION

Concrete is widely used construction material for civil and protection structures. Owing to its customizable mechanical properties and cost-effectiveness, concrete has become the effective choice for the construction of bunkers and field fortifications. The defeat of a concrete target is generally brought about by kinetic energy projectiles. However, low-velocity missiles and projectiles that cannot penetrate hard concrete targets may employ follow-through warheads in which a precursor shaped charge warhead weakens the target. In such situations, a large crater in concrete target by precursor shaped charge warhead is desirable for enabling the entry of the following projectile containing a sufficient quantity of explosive to neutralise the target. The shaped charge warhead produces a hypervelocity jet by the collapse of a metallic liner under explosive action. The jet must produce maximum damage in the target for the follow-through penetrator to pass through.

Numerous researchers have studied penetration into concrete targets by hypervelocity jets that erode during the penetration process. These studies are mostly on the local damage characteristics like depth of penetration and crater diameter. Kalia[1] has reported on various liner materials and their metallurgical aspects that give deeper penetration into granite. Held[2] correlated penetration of shaped charge jet into

sand and concrete with hydrodynamic theory. He observed that penetration depths by shaped charge jets into concrete are approximately 2.7 times that in steel targets and that low-velocity portions of the jets were also useful in penetrating the concrete. Held carried out these studies using Copper liners. Fundamental theories of hydrodynamic penetration state that the higher the density of the jet, the deeper is the penetration with a smaller borehole diameter. Murphy and Kuklo[3] investigated several relations that correlate concrete target damage to the shaped charge warhead and target configuration. They observed that the borehole diameter from the Aluminium jet is larger than that from Copper jets. Gold[4], *et al.* investigated the penetration characteristics of Copper and Tantalum eroding projectiles in concrete as a function of impact velocity and concrete reinforcement. Impact velocities of projectiles were 1.5 – 1.9 km/s. Murphy[5] has presented a unified approach of modelling shaped charge jet formation and concrete target penetration using analytical models. Nia[6], *et al.* confirmed the hydrodynamic model of penetration in semi-infinite concrete targets by eroding rod penetrators. He observed that the effect of heterogeneity in concrete is reduced by the increase of impact velocity beyond the hydrodynamic regime. The hydrodynamic theory provides a very good approximation to the depth of concrete penetration by eroding projectiles; however, it does not capture the extent of peripheral damage or loss of tensile strength of bulk target material beyond the crater formed by the projectile.

Islam[7], *et al.,* have presented a numerical analysis of high-velocity penetration of ogive-nosed steel projectiles into concrete targets at impact velocities around 1200m/s. The authors were able to capture the failure patterns i.e., the entry side crater and exit side spall failure, observed in actual experiments. Nystrom and Gylltoft[8] used numerical hydrocode Autodyn™ to extensively study the influence of reinforcement on crater formation and crack propagation beyond the crater. These numerical studies were carried out for impact velocities of 485m/s and 650m/s. Lu[9], *et al.* reported the mechanism for front face crater formation due to projectile impact. The damage is a combined effect of compression and tensile failure of the material. Kong[10], *et al.* presented a modified Alekseevskii-Tate model combining one-dimensional target resistance to predict the depth of penetration by eroding projectiles. Recent studies by Zhu[11], *et al.*, bring out the depth of penetration and radial cavity growth caused by shaped charge jet penetration in ultra-high-strength concrete.

Penetration of concrete targets by eroding penetrators has been studied by many researchers as given above. However, there is not much work published on the effect of the penetrator erosion rate, the target-penetrator interface velocity and the impact energy partitioning on the crater characteristics, when different penetrator materials are employed against concrete target. These parameters are important for the selection of penetrator material for inflicting maximum damage to concrete targets. Hence the objective of this paper is to numerically study the influence of eroding penetrator material on the penetration characteristics and the damage inflicted to concrete targets beyond the crater formed by the penetrator. Penetration crater volume in the target depends upon the energy imparted to the target by the projectile. The kinetic energy imparted to the target by the projectile is partitioned into internal energy and kinetic energy of the target. Hypervelocity projectiles deposit energy into the target while eroding hydrodynamically. The rate of erosion of the projectile depends on the impact velocity and its material. Erosion of projectiles strongly influences the crater characteristics. This paper is also aimed at studying the effect of target thickness on the lateral extent of its damage. The erosion rate of impacting projectiles in combination with target thickness, whether finite or infinite, determines the amount of energy deposited in the target. If the projectile is not fully eroded by the time when the target is perforated, much of the energy will be carried away by the residual projectile thereby depositing lesser energy in the target. This fact is important for choosing the right projectile material for defeating finite concrete targets.

2. METHODOLOGY

Tate and Alekseevskii have modified the Bernoulli equation to include the strength terms for modelling long-rod penetration in semi-infinite targets[12]. Accordingly, the pressure at the interface of the projectile and the target is given as:

$$\frac{1}{2}\rho_p \left(v-u\right)^2 + Y_p = \frac{1}{2}\rho_t \left(u\right)^2 + R_t \tag{1}$$

when R_t approaches Y_p, the hydrodynamic limit of penetration is reached. The normalised penetration at the hydrodynamic limit is, $S_h = \left(\dfrac{\rho_p}{\rho_t}\right)^{1/2}$. Figure 1 provides a schematic of the projectile and target impact scenario.

Numerical simulations have been carried out to study the penetration characteristics in concrete using penetrators made of three different materials, viz, Iron-ARMCO, Copper-OFHC, and Aluminium-6061 impacting at hyper velocities. 2D axisymmetric analysis was performed. Penetrator and target are modelled as cylindrical rods. In all the cases, the same amount of kinetic energy was imparted to the target to study the penetration characteristics. Length and diameter of penetrator have been kept the same and velocity has been varied to achieve the same value of kinetic energy. A detailed test matrix is given in Table 1. The diameter of the target
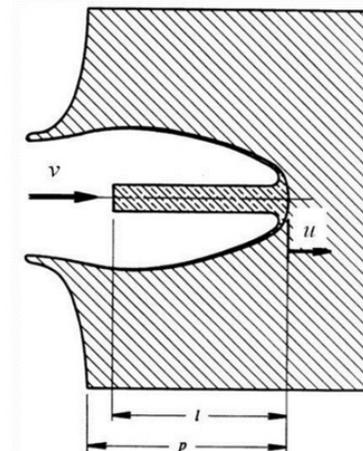

Figure 1. Schematic representation of eroding rod penetration[13].

is sufficiently large so that the effect of reflected shocks from the free boundary on the penetration process is negligible. The velocity of the penetrator-target interface, u, during the penetration process is observed in each case. This indicates the hydrodynamic nature of penetration. The tail velocity of the penetrator is plotted to see projectile deceleration during penetration. Plastic strain contours around the crater are a measure of damage in the concrete target. The extent of plastic strain contour for different penetrator materials is plotted as they deposit the same amount of energy in the target. When the penetrator impacts the target, the kinetic energy of the penetrator is converted into kinetic energy and internal energy of the target. Plots of energy partitioning explain the rate of energy delivery into the target by the projectile and distribution and dissipation of energy within the target.

Table 1. Test Matrix for simulations

Penetrator material	Diameter, (mm)	Length, (mm)	Density, (g/cc)	Mass, (g)	Velocity, (m/s)	Kinetic Energy, (J)
Aluminium	20	100	2.70	84.823	3000.0	381703.51
Iron	20	100	7.89	247.872	1755.0	381725.98
Copper	20	100	8.93	280.544	1649.6	381705.38

Table 2. S-G constitutive constants

Penetrator material	Model	Y_0 (GPa)	G_0 (GPa)	β	n	Y_p'	G_T' (GPa/K)	η
Aluminum	S-G	0.29	276	125	0.1	0.02	-0.017	1
Copper	S-G	0.12	477	36	0.45	0.0034	-0.017	1

Table 3. J-C constitutive constants

Penetrator material	Model	A (GPa)	B (GPa)	C	n	m	T_m (K)
Iron	J-C	0.175	0.38	0.06	0.32	0.55	1811

Tables 2 and 3 provide the constitutive parameters for the three penetrator materials considered for this study.

Johnson-Cook model

$$\sigma_{eq} = \left[A + B\varepsilon_p^n \right]\left[1 + C\ln\left(\frac{\dot{\varepsilon}_p}{\dot{\varepsilon}_0}\right)\right]\left(1 - \theta^m\right);$$

$$\dot{\varepsilon}_0 = 1.0 s^{-1}; \theta = \frac{T - T_0}{T_m - T_0}; T_0 = 300°K$$

(2)

Steinberg – Guinan model

$$\sigma_{eq} = Y_0\left(1 + \beta\varepsilon_p\right)^n \left\{1 + \left(\frac{Y_p'}{Y_0}\frac{P}{\eta^{\frac{1}{3}}}\right) + \frac{G_T'}{G_0}\left(T - 300\right)\right\}$$

(3)

Micro cracking experienced by concrete during the dynamic loading process leads to a reduction in strength and stiffness[17]. These hypotheses are considered in the RHT constitutive model of concrete. The model parameters for concrete having 35MPa compressive strength are presented in Table 4.

3. NUMERICAL MODEL

The 2-D eulerian wave propagation code Autodyn-2D™ was used to perform the numerical experiments. Penetrator and target were considered axisymmetric.

A benchmarking was carried out to confirm the meshing effectiveness by validating the experimental study carried out by Dawson[14]. Tungsten alloy penetrators of length 94.6 mm and diameter 6.25 mm were impacted on plain cement concrete target at a velocity of 2.26 km/s. Experimental results like penetration depth, crater diameter and residual velocity of penetrator were simulated to less than 5% error from reported experimental values et al.. Accordingly, square zoning with a constant cell dimension of 0.5mm was used for the calculations.

Constitutive response of the projectile materials was represented by the Johnson-Cook (J-C) model for Iron whereas Copper and Aluminium have been represented by Steinberg-Guinan (S-G) model. The applicability of the S-G model for Aluminium and Copper has been confirmed by Peng[15], *et al.*, under temperature and shock pressures. However, the Taylor impact study by Banerjee[16] has revealed that the S-G model fails in the case of steel for high impact velocities. J-C model, though not very accurate at high temperatures, captures rate dependent effects quite well. Compressibility effects can be neglected as the density of target and penetrator do not change during the penetration process.

4. RESULTS

4.1 Phases of Penetration and Penetration Velocity

Penetration occurs during the steady-state is called the primary phase and the remaining penetration is known as secondary penetration[18]. The penetration velocities, u, for the

Table 4. Values and parameters for RHT Concrete model

Parameter	Value	Parameter	Value	Parameter	Value
Reference density, g/cm³	2.75	A1 (kPa)	3.527E+7	Specific heat, (J/kgK)	6.54E+2
Porous density, g/cm³	2.314	A2 (kPa)	3.958E+7	Shear Modulus, (kPa)	1.67E+7
c_{porous}, m/s	2920	A3 (kPa)	9.040E+7	Compressive Strength, f_c, (kPa)	3.5E+4
Solid EOS	Polynomial	B0 (kPa)	1.22	f_t/f_c	0.1
Compaction curve	Standard	B1 (kPa)	1.22	f_s/f_c	0.18
Initial compaction pressure, kPa	2.33E+4	T1 (kPa)	3.527E+7	A_{fail}	1.6
Solid compaction pressure, kPa	6.0E+6	T2 (kPa)	0	N_{fail}	0.61
Compaction exponent	3.0	T_{ref} (K)	300	Tensile failure model	Hydro

different combinations of target and penetrator show that the penetration progresses close to hydrodynamic velocity but slightly below the hydrodynamic limit. They are plotted in Fig. 2. It is due to the strength effects the penetration velocity drops below the hydrodynamic limit as given by equation 1. It can also be seen that steady-state penetration is completed even before the hydrodynamic penetration limit is reached. The secondary penetration governed by the inertial effects set the target in motion after the penetrator is completely eroded. This secondary penetration allows the penetration to continue beyond hydrodynamic limits. A closer examination of the plots reveals that the Aluminium penetrator has a steady penetration velocity throughout its penetration in concrete. The proportion of secondary penetration is maximum when the target is penetrated with an Aluminium penetrator as compared to the other two materials. This is because the Aluminium penetrator sets the target into motion with higher velocities even after the steady-state penetration is completed owing to its higher impact velocities. The motion of target material by the projectile penetration results in plastic strain and loss of strength of the target. Hence for the same input energy, an Aluminium penetrator would cause more lateral damage in concrete as compared to copper or iron penetrators.

4.2 Penetrator Deceleration

Multiple reflections of elastic waves occur between the tail end of the penetrator and the target/penetrator interface during the penetration process. These decelerations cause the penetrator to decelerate. Figure 3 depicts the variation of tail velocities to penetration time. Iron shows larger deceleration when penetrating concrete as more elastic reverberations are possible owing to its lower velocities as compared to the Aluminium penetrator. Moreover, strength effects are more predominant in the case of the Iron penetrator and a steady state of penetration is completed in the early stages of penetration itself. Aluminium and Copper penetrators have a nearly steady tail velocity indicating a steady penetration process.

4.3 Plastic Strain Contour

Contours of equivalent plastic strain are shown in Fig. 4 for the three cases studied. These figures are plotted when the penetrator has completely eroded. The impact craters are approximately cylindrical. Plastic strain contours provide a measure of the extent of damage in the concrete target. As seen from these plots, the lateral extent of plastic strain in concrete is more in the case of an Aluminium penetrator. The interface pressure during the penetration process reveals that though the magnitude of pressure is higher for Aluminium, the duration of the same is much less as the penetration process is quickly completed due to faster erosion of the Aluminium penetrator. Interface pressure values for the three penetrators when they penetrate concrete are shown in Fig. 5. When the steady-state penetration ends, the interface pressure starts reducing because the process is governed mostly by the secondary penetration.
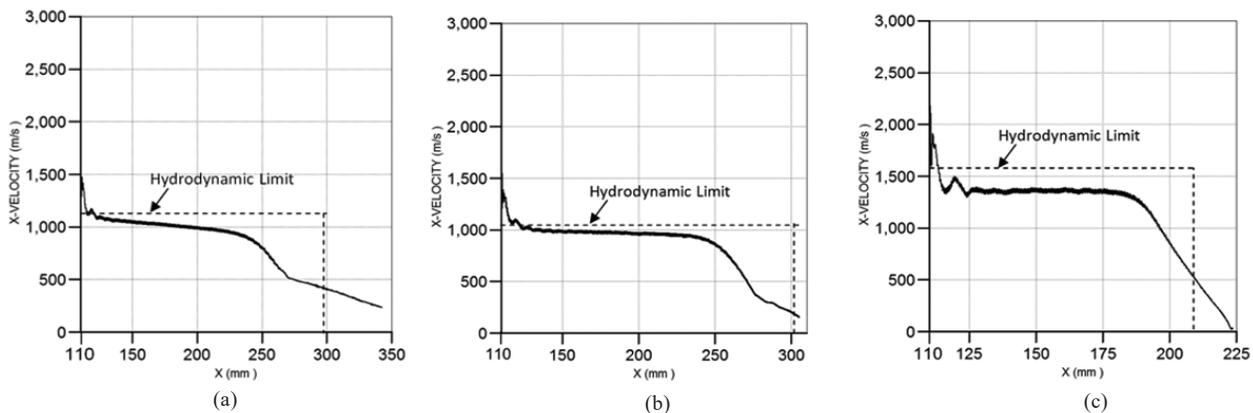

Figure 2. Penetration velocities versus depth of penetration (a) Iron penetrator, (b) Copper penetrator, and (c) Aluminium penetrator.
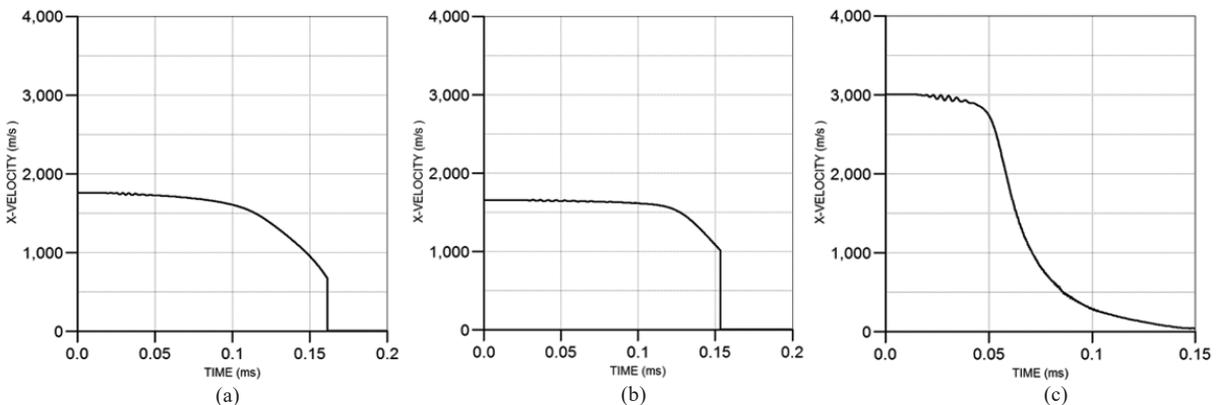

Figure 3. Tail velocities versus penetration time (a) Iron penetrator, (b) Copper penetrator, and (c) Aluminium penetrator.
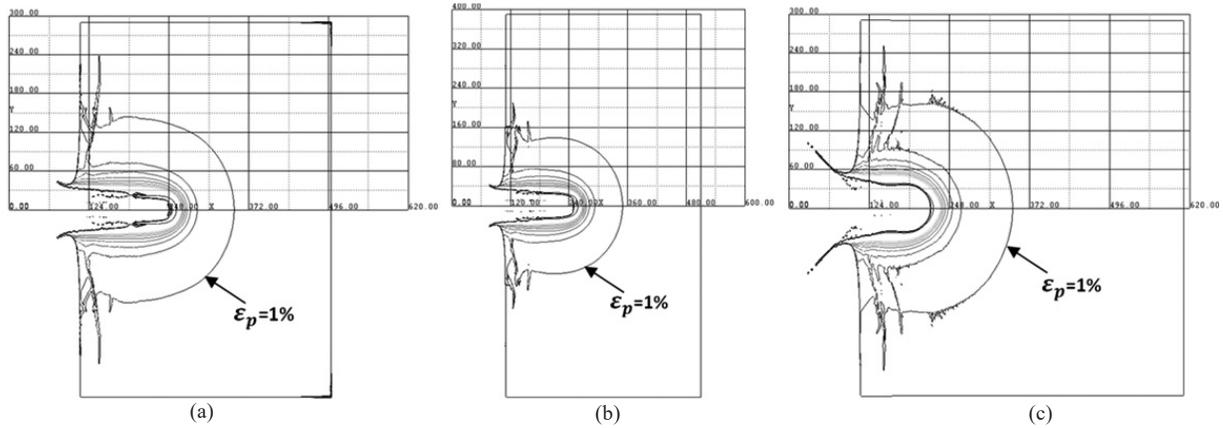
Figure 4. Plastic strain contours during the penetration process (a) Iron penetrator, (b) Copper penetrator, and (c) Aluminium penetrator.
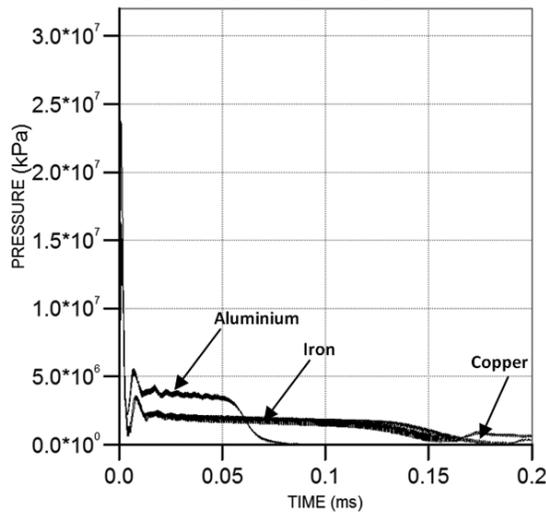

Figure 5. Interface pressure for aluminium, iron and copper penetrators.

During the secondary penetration process, the interface pressure is almost absent. In the case of the Aluminium penetrator, the penetration process ceases early as erosion of the penetrator is more. However, for the same energy deposited into the target, lateral expansion of plastic strain contours is more

for the Aluminium penetrator. 1% of plastic strain is taken as the extent of the plastic zone in this study. The extent of the plastic zone is the work done by the projectile on the target. The plastic zone increases both axially and radially during the penetration process. Penetration velocity for Aluminium penetrator is more than that of Iron and Copper penetrator. As Aluminium erodes faster, the depth of penetration is less. However, the energy deposited in the target expands the plastic zone laterally.

4.4 Energy Partitioning

Figure 6 shows the energy partitioning in the process of three different penetrators penetrating the concrete target. Four curves are shown in each subfigure.

As the penetration progresses, the kinetic energy of the penetrator reduces linearly with time. This is because the length of the penetrator reduces linearly during the penetration process. It may be recalled that all the three penetrators have identical kinetic energy at the time of impact and it is converted into internal and kinetic energy of the target. The kinetic energy received by the target is dependent on the penetrator velocity. Hence in the present case, the Aluminium penetrator imparts maximum peak kinetic energy to the target. At around 0.06ms, the Aluminium penetrator completely erodes and a considerable
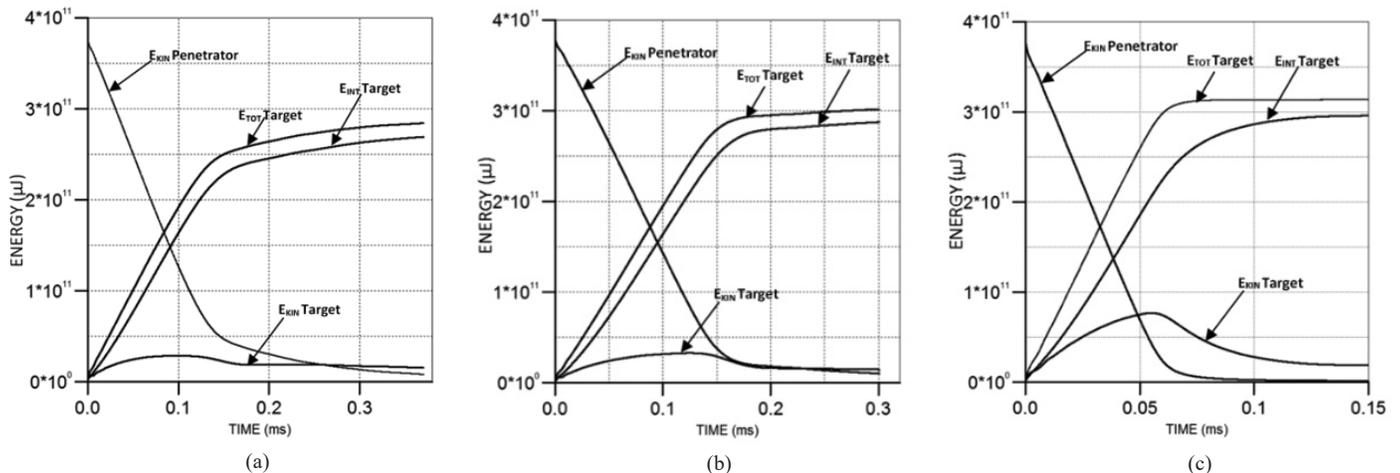

Figure 6. Energy partitioning versus time of penetration: (a) Iron penetrator, (b) Copper penetrator, and (c) Aluminium penetrator.
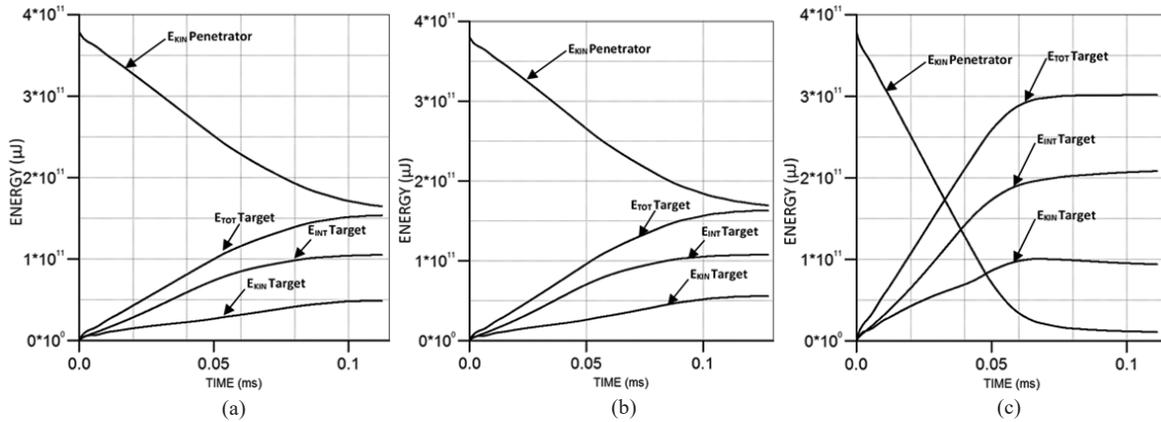
Figure 7. Energy partitioning versus time of penetration-Finite target thickness: (a) Iron penetrator, (b) Copper penetrator, and (c) Aluminium penetrator.

amount of kinetic energy is still present in the target. The kinetic energy received by the target is quickly converted to internal energy which manifests as the plastic strain in the target. In the case of penetration by the Aluminium rod, the lateral extent of plastic strain is more than the axial extent as the total penetration is lesser than the other two projectiles.

4.5 Energy Partitioning in Case of a Target with Finite Thickness

A case has been studied where the above-considered penetrators were impacted on the finite thickness of the concrete target. Target thickness has been restricted exactly to the length of the penetrator. In the present case, all the penetrators are of an equal length of 100mm. Since the hydrodynamic penetration limit for Aluminium penetrator in concrete target is close to the penetrator length, it completely erodes when the thickness of the target is penetrated. Therefore, the Aluminium penetrator deposits total energy possessed by it to the target. However, Copper and Iron penetrators exit the target before completely getting eroded. Hence, only a fraction of its kinetic energy is deposited in the target. This aspect is clear from Fig. 7 where energy partitioning for a finite thickness target is depicted. Accordingly, an Aluminium penetrator with the same kinetic energy as that of Iron or Copper penetrators inflicts maximum damage to the concrete target when the target thickness is finite.

5. CONCLUSIONS

A numerical simulation study has been carried out to understand the concrete penetration characteristics of eroding rods of identical dimensions and made of three different materials viz., Iron, Copper, and Aluminium *when impacted with the same amount of kinetic energy*. Major observations and findings are listed below:

5.1 Interface Pressure

Penetrator-target interface pressure depends on the density of penetrator and square of the impact velocity. Impact velocities are more for the Aluminium penetrator for achieving the identical impact energy as that of Copper and Iron penetrators. Hence the target-penetrator interface pressure is maximum in case of Aluminium penetrator.

5.2 Hydrodynamic Penetration

Copper penetrator shows a nearly hydrodynamic penetration process in concrete for the given velocity. The case of Copper penetrator impacting Concrete target has the lowest hydrodynamic limit out of all the combinations considered. In all the three cases, penetration velocity is a little below the hydrodynamic limit implying the effect of strength in the penetration process. In the case of Aluminium penetrator, penetration velocity is highest owing to the high impact velocity. However, it has maximum deviation from hydrodynamic limit. Hydrodynamic theory can be used to give a reasonably good approximation for the eroding rod penetration in concrete though the steady-state penetration stops before reaching the hydrodynamic limit. Secondary penetration makes it possible to reach the hydrodynamic limit of penetration. Secondary penetration is due to the inertia effect of the target after the penetrator is completely eroded. The penetration velocity drops faster and becomes unsteady in the case of the Iron penetrator. This is because deformation energy per unit volume for Iron is more as compared to Copper and Aluminium. More energy is consumed in deforming the Iron penetrator as compared to the other two materials.

5.3 Lateral Damage

Lateral damage in concrete is more when penetrated by an Aluminium penetrator. Deformation energy per unit volume is less for the Aluminium penetrator hence total energy deposited in the target is more. The penetration borehole with aluminum penetrator is larger in diameter, while a deeper depth of penetration is obtained by the other two penetrators. In the case of finite thickness of concrete target, the Aluminium penetrator inflicts maximum lateral damage as the total kinetic energy of the penetrator is delivered to the target.

REFERENCES
1. Kalia, H.N. Penetration in granite by shaped charge liners of various metals, University of Missouri-Rolla, USA, 1970. (PhD Thesis). https://scholarsmine.mst.edu/doctoral_dissertations/2038 [Accessed on 03-01-2021]
2. Held M. Refined shaped charge jet penetration measurement in various materials versus hydrodynamic prediction. *In* Proceedings of the 10th International

Symposium on Ballistics, San Diego, CA, USA, 1987.

3. Murphy, M.J. & Kuklo, R.M. Fundamentals of Shaped Charge Penetration in Concrete. *In* Proceedings of the 18th International Symposium on Ballistics, San Antonio, TX, USA, 1999.

4. Gold, V. M.; George C.V. & James C.P. Concrete penetration by eroding projectiles: Experiments and analysis. *J. Eng. Mech.*, 1996, **122** (2),145-152.
doi: 10.1061/(ASCE)0733-9399(1996)122:2(145)

5. Murphy, M.J. Shaped charge penetration in concrete: A unified approach., University of California, Davis, USA, 1983. (PhD Thesis).

6. Nia, A.A; Zolfaghari, M.; Khodarahmi, H.; Nili, M. & Gorbankhani, A.H. High-Velocity Penetration of Concrete Targets with Eroding Long- Rod Projectiles; An Experiment and Analysis. *Int. J. Prot. Struct.*, 2014, **5**(1), 47-63.
doi: 10.1260/2041-4196.5.1.47

7. Islam, M. J.; Liu, Z. S. & Swaddiwudhipong, S. Numerical study on concrete penetration/perforation under high-velocity impact by ogive-nose steel projectile.
Comput. Concr., 2011, **8**(1), 111–123.
doi: 10.12989/cac.2011.8.1.111

8. Nyström U. & Gylltoft K.; Comparative numerical studies of projectile impacts on plain and steel-fibre reinforced concrete. *Int. J. Impact Eng.,* 2010, **38**(2-3), 95-105.
doi: 10.1016/j.ijimpeng.2010.10.003

9. Lu, Y.; Zhang, Q.; Xue, Y.; Shang, C.; Liu, W.; Ren, S. & Long, R. Hypervelocity impactcratering on semi-infinite concrete targets of projectiles with different length to diameter ratios. *Appl. Sci.* 2020, **10**(11), 3910.
doi: 10.3390/app10113910

10. Kong, X.Z.; Wu, H.; Fang, Q. & Peng, Y. Rigid and eroding projectile penetration into concrete targets based on an extended dynamic cavity expansion model. *Int. J. Impact Eng.,*2017, 100, 13-22.
doi: 10.1016/j.ijimpeng.2016.10.005

11. Zhu, Q.; Huang, Z.; Xiao, Q.; Zu, X. & Jia, X. Theoretical and experimental study of shaped charge jet penetration into high and Ultra-high strength concrete targets. *Int. J. Impact Eng*, 2018,122, 431-438.
doi: 10.1016/j.ijimpeng.2018.04.010

12. Anderson, C.E. & Walker, J.D. An examination of long-rod penetration. *Int. J. Impact Eng.*, 1991,**11**(4), 481-501.
doi: 10.1016/0734-743X(91)90015-8

13. Anderson, C.E.; Orphal, D.L.; Franzen, R.R. & Walker, J.D. On the hydrodynamic approximation for long-rod penetration. *Int. J. Impact Eng.*,1999, **22**(1), 23-43.
doi: 10.1016/S0734-743X(98)00044-X

14. Dawson, A; Bless, S.; Levinson, S.; Pedersen, B. & Satapathy, S. Hypervelocity penetration of concrete. *Int. J. Impact Eng.*, 2008, **35**(12),1484-1489.
doi: 10.1016/j.ijimpeng.2008.07.069

15. Peng, J.; Jing, F.; Li, D. & Wang, L. Pressure and temperature dependence of shear modulus and yield strength for aluminum, copper, and tungsten under shock compression. *J. Appl. Phys*. 2005, **98**(1), 013508.
doi: 10.1063/1.1943510

16. Banerjee, B. Validation of the material point method and plasticity with Taylor impact tests.
arXiv:1201.2476 [physics.comp-ph] [Accessed on 03-01-2021]

17. Tham, C.Y. Reinforced concrete perforation and penetration simulation using AUTODYN- 3D. *Finite Elem Anal Des.*, 2005, **41**(14), 1401-1410.
doi: 10.1016/j.finel.2004.08.003

18. Anderson, C.E.; Littlefield, D.L. & Walker, J.D. Long-rod penetration, target resistance, and hypervelocity impact. *Int. J. Impact Eng.*, 1993, **14**(1–4), 1-12.
doi: 10.1016/0734-743X(93)90004-Q

CONTRIBUTORS

Mr S. Harikrishnan received his BTech (Mechanical Engg.) from Kerala University and MTech (Machine Design) from IIT Madras. Currently, he is serving as Scientist G in DRDO-ARDE, Pune. His area of specialisation is the design and development of warheads for missiles, torpedoes, and ammunition. He has been associated with the development of warheads for the Integrated Guided Missile Development Programme (IGMDP) and other missile systems.
In this paper, he planned and carried out various simulation studies and prepared the manuscript.

Dr V. Venkateswara Rao obtained his PhD from JNTU, Hyderabad. He has served as Programme Director AGNI and Director, Center for Advanced Systems. Currently, he is serving as Outstanding Scientist and Director, ARDE, Pune. He has immensely contributed towards the integration and testing of solid rocket motors for various missile systems. He has to his credit, several technical papers published in national and international journals and conference proceedings. He is the recipient of various awards including the DRDO award for path-breaking research and the best performance team award. He was awarded the Best PhD thesis award by the Indian Welding Society in 2010.
In this paper, he has guided the author and reviewed the manuscript.

Dr Ajay Misra obtained his MTech from IIT Bombay and PhD from IIT Kanpur. He is currently working as Head of the Department of Aerospace Engineering at Defence Institute of Advanced Technology, Pune. His areas of interest are Flight Control and Guidance, Cascade Fins, Shockwave, and boundary layer interaction, and Hypervelocity projectile penetration mechanisms. He has published several research papers in peer-reviewed journals. He is the recipient of the Best Professor Award-2018 from the Society of Aeronautical Engineers (India).
In the present work, he has guided the author, reviewed, and formatted the manuscript.